

# Aeromagnetic 3D subsurface imaging with effective source volume minimization and its application to data from the Otoge cauldron, Shitara, Central Japan

Tadashi Nakatsuka<sup>1</sup> Shigeo Okuma

Geological Survey of Japan, AIST, 1-1-1 Higashi, Tsukuba, 305-8567 Japan

<sup>1</sup>E-mail: [tad.nktk@ni.aist.go.jp](mailto:tad.nktk@ni.aist.go.jp)

**Key Words:** aeromagnetic anomaly, 3D imaging, conjugate gradient method, compact inversion, effective volume minimization, Otoge cauldron, magma reservoir

## ABSTRACT

Three-dimensional (3D) imaging techniques using the conjugate gradient solution are discussed for magnetic anomaly source reconstruction, especially for rugged terrain areas such as those of volcanoes. The analysis model configuration permits surface undulation and variable depth slicing. First, primitive source model data are put into the analysis to confirm the characteristic behaviour of the regularization methods and parameter scaling. The compact regularization method is then applied to synthetic geologic models to understand the resolving power of the method given the problem of the inherent weakness of a non-unique solution. Finally, the field data of a helicopter-borne magnetic survey of the Otoge cauldron are put into the 3D imaging analysis with the method. The analysis reveals a quite reasonable subsurface image of the magma reservoir and the Otoge cone sheets and Otoge stocks of post-cauldron activity, as inferred from geological studies.

## INTRODUCTION

Recent developments in aeromagnetic surveying, including improved accuracy of position fixing and navigation, have enabled us to detect more details of subsurface structure. High-resolution aeromagnetic survey using a helicopter has become more popular, especially in areas of volcanic activities. Magnetic survey flights by helicopter are usually executed parallel to the topographic surface, but the altitudes of observation may be too variable to be regarded as a smooth surface. The commonly used equivalent source technique has been proven to provide an efficient means of altitude reduction (Nakatsuka and Okuma, 2006a),

which led us to the technology of detecting temporary magnetic anomaly changes (Nakatsuka and Okuma, 2006b; Nakatsuka *et al.*, 2009).

For interpreting magnetic anomalies in terms of subsurface magnetic structure, we have often used the method of magnetization intensity (two-dimensional) mapping (Okuma *et al.*, 1994; Nakatsuka, 1995; Okubo *et al.*, 2006). The technology of three-dimensional (3D) imaging is theoretically a straightforward step from the magnetization-intensity mapping. Since Li and Oldenburg (1996) and Pilkington (1997) developed their 3D inversion technique, we also have been developing our software for 3D subsurface imaging (Okuma *et al.*, 2009). As is well known, magnetic (potential field) anomaly data cannot, in theory, provide a unique solution of subsurface structure, and there are infinite possibilities of equivalent 3D sources. Therefore, some constraint on the source distribution is necessary to obtain a valid result, and the result must be inspected for plausibility. Unless another type of observation is available for a unified interpretation of multidisciplinary data, some philosophical strategy must be developed to overcome the difficulty.

Earth sciences can be thought of as the branch of science that deals with obtaining knowledge of nature by simplifying a complex and diverse situation. A minimum norm solution is one candidate and is effective for the underdetermined solution of magnetization intensity mapping (Nakatsuka, 1995). In the simple synthetic study of 3D imaging, however, it has been proven that a minimum norm criterion cannot provide a

focused image of subsurface structure but tends to result in a broader source shape with a vague boundary, especially toward the deeper part, as an equivalent source model. Smoothness (minimum roughness) regularization, as is often used in non-linear problems, such as in EM methods (e.g., Uchida, 1993), seems to have a similar character. We here adopt the compactness criterion, as developed by Last and Kubik (1983) and Portniaguine and Zhdanov (1999, 2002), to obtain a localized source image from observation.

Recent developments in this field have focused on new ideas of regularization techniques and the artifice of reducing the practical matrix size so as to be handled in the calculation (e.g., Silva *et al.*, 2007; Pilkington, 2009). Most of these use a regular source distribution of voxels, which may not be favourable for our application in an area of undulating topography. Instead, we want to develop a model configuration accommodated to the rough terrain and observation surfaces of a mountainous area and omit unnecessary fine division of source elements given the natural degradation of resolving power with depth.

## ANALYSIS MODEL FOR 3D IMAGING

First, we would like to describe the analysis model we used in this study. As we are aiming for application of 3D imaging to helicopter-borne magnetic surveys in mountainous regions, such as active volcanoes, our model configuration has a surface undulation and variable depth slicing, as shown in vertical section view in Fig. 1. There are two options for defining the model configuration: (a) horizontal layer slicing, and (b) constant burial depth slicing (variable thickness layer by layer).

We here introduced an additional source zone around the area of observation to avoid the edge effect (Nakatsuka, 1995; Nakatsuka and Okuma, 2006a). As the analysis results in this zone of surrounding sources (away from the observation) is not very reliable, we will generally mask them in the result illustration.

In this research, we deal with the total intensity magnetic anomalies observed at a certain clearance above the terrain over a mountainous area. As is widely done, we also assume that the total intensity anomaly is well approximated by the projection of the vector anomaly to the ambient field direction. If any greater anomaly amplitude exists, violating the assumption, we should

further consider the projection of anomalous field vector onto the ambient field direction (Clark, 2013, Appendix A). We also use a model with invariant direction of source magnetization because too loose a constraint on the physical situation in an underdetermined problem may result in an ill-posed problem.

## ALGEBRA OF 3D IMAGING

The basic formula of 3D subsurface imaging is completely identical to equivalent source analysis (Nakatsuka and Okuma, 2006a) and magnetization intensity mapping (Nakatsuka, 1995), but the sources are distributed in three-dimensional space and have the physical quantity of magnetization. The magnetic anomaly  $f(\mathbf{p})$  at the observation point  $\mathbf{p}$  is expressed as

$$f(\mathbf{p}) = \int_Q A(\mathbf{p}, \mathbf{q}) s(\mathbf{q}) ds \quad , \quad (1)$$

where  $s(\mathbf{q})$  is the magnetization of a source located at  $\mathbf{q}$ , and  $A(\mathbf{p}, \mathbf{q})$  is the source effect coefficient (geometric factor) combining  $f(\mathbf{p})$  with  $s(\mathbf{q})$ .

Using vector/matrix notation, a discrete form of original Equation (1) can be expressed as

$$\mathbf{f} = \mathbf{A}\mathbf{s} \quad . \quad (2)$$

Here, the formula of the magnetic anomaly of a prism-shaped source body (e.g., Bhattacharyya, 1964) is used to calculate the geometric factor  $\mathbf{A}$ , but it may be alternated with the formula of a point source model if the mesh of the source distribution is sufficiently fine.

## Conjugate Gradient Method and Regularization

As Equation (2) is linear, the problem seems quite simple. However, there exists the problem of the number of unknown parameters, e.g.,  $10^5$  to  $10^8$  or more, and the problem of being underdetermined, i.e., the number of unknown parameters  $\mathbf{s}$  exceeds the effective number of observation data  $\mathbf{f}$ . Nakatsuka and Okuma (2006a) and Nakatsuka (1995) solved such problems by the conjugate gradient (CG) method. The CG method as applied to an underdetermined linear problem gives a minimum

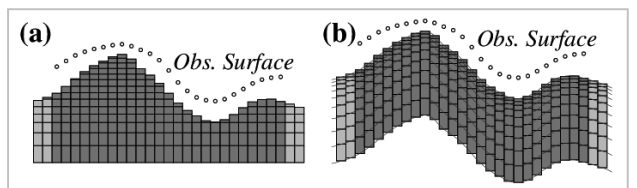


**Fig. 1 Two types of layer configuration (section view) for 3D magnetization imaging software: (a) horizontal layer slicing, and (b) constant burial depth slicing (variable thickness layer by layer).**

Euclidean norm solution (Nakatsuka, 1995) if begun from a null source, or the solution falls into the one nearest to the starting model.

To solve Equation (2), the simple CG method searches for the condition

$$(\mathbf{f} - \mathbf{As})^T (\mathbf{f} - \mathbf{As}) \rightarrow \text{Min} , \quad (3)$$

which corresponds to the normal equation,

$$\mathbf{A}^T \mathbf{f} = \mathbf{A}^T \mathbf{As} . \quad (4)$$

The CG method procedure that we used to solve Equation (2) is described in Fig. 2.

However, the result from the simple CG solution cannot provide a focused image of subsurface structure, as is illustrated later. As favourable solutions for such a problem, various methods of regularization are utilized. The generalized formulation for these is given as follows.

In case of regularization methods, an additional term is introduced in the minimizing function as

$$(\mathbf{f} - \mathbf{As})^T (\mathbf{f} - \mathbf{As}) + e(\mathbf{Bs})^T (\mathbf{Bs}) \rightarrow \text{Min} , \quad (5)$$

where  $\mathbf{B}$  is the penalizing operator matrix, and  $e$  is a trade-off parameter to adjust the penalizing weight ratio between the former misfit term  $(\mathbf{f} - \mathbf{As})^T (\mathbf{f} - \mathbf{As})$  and the latter regularization term  $R = (\mathbf{Bs})^T (\mathbf{Bs})$  in (5). This formulation (5) corresponds to the normal equation for the combined equation

$$\begin{bmatrix} \mathbf{A} \\ \sqrt{e}\mathbf{B} \end{bmatrix} \mathbf{s} = \begin{bmatrix} \mathbf{f} \\ \mathbf{0} \end{bmatrix} , \quad (6)$$

and the application of the simple CG method to this equation is reduced to obtaining the regularized solution for Equation (2).

If a unit matrix is selected for  $\mathbf{B}$ , the formulation (5) means the minimum norm regularization. Similarly, if  $\mathbf{B}$  is a Laplacian (roughness operator) matrix, the problem is reduced to smooth inversion.

### Compactness Regularization

Last and Kubik (1983) first introduced a compact inversion technique in a 2-D gravity analysis, and Portniaguine and Zhdanov (2002) developed it into 3-D magnetic imaging. The idea is to adopt the penalizing operator matrix as

$$\mathbf{B} = \text{diag} \left\{ 1 / \sqrt{s_i^2 + \delta^2} \right\} , \quad (7)$$

```

Procedure of CG method to solve  $\mathbf{f} = \mathbf{As}$ 
Preparation: Define parameter scaling factor  $\mathbf{C}^2$ 
              (Diagonal matrix, Unit matrix when no scaling)
Start: Give initial values  $s_0$  ( $\mathbf{0}$  if no a priori info.)
 $k := 0$ ,  $r_0 := \mathbf{f} - \mathbf{As}_0$ ,  $u_0 := \mathbf{A}^T r_0$ 
 $e_0 := u_0^T \mathbf{C}^2 u_0$ ,  $p_0 := \mathbf{C}^2 u_0$ 
Do loop {
   $q_k := \mathbf{A} p_k$ ,  $\alpha_k := e_k / (q_k^T q_k)$ 
  Increment  $k$  ( $k := k+1$ )
   $s_k := s_{k-1} + \alpha_{k-1} p_{k-1}$ ,  $r_k := r_{k-1} - \alpha_{k-1} q_{k-1}$ 
  Exit loop if converged
   $u_k := u_{k-1} - \alpha_{k-1} \mathbf{A}^T q_{k-1}$ ,  $e_k := u_k^T \mathbf{C}^2 u_k$ 
   $p_k := \mathbf{C}^2 u_k + (e_k / e_{k-1}) p_{k-1}$ 
}
Solution:  $s_k$ , misfit:  $r_k$ 

```

**Fig. 2** Conjugate gradient procedure for solving simultaneous linear equations (with/without parameter scaling). ‘:=’ indicates that the left-hand variable is substituted by the calculation result of the right-hand expression. The RMS misfit is monitored to judge if the solution converges to an exit loop. In actual program coding, when the percentage of improvement in RMS misfit is less than the specified value for five continuous iterations or the RMS misfit is less than 0.1 nT, the loop iteration is terminated.

and the regularizing term  $R$  becomes

$$R = (\mathbf{Bs})^T (\mathbf{Bs}) = \sum_i \frac{s_i^2}{s_i^2 + \delta^2} . \quad (8)$$

Here  $\delta (> 0)$  is a critical value of magnetization, and source bodies with small magnetization well below  $\delta$  ( $|s_i| \ll \delta$ ) are regarded as being ineffective for building up anomalies. As each element of  $R$  has a value between 0 ( $|s_i| \ll \delta$ ) and 1 ( $|s_i| \gg \delta$ ), the minimization of  $R$  corresponds to the minimization of the number of sources contributing to the anomaly build up. This is equivalent to minimizing source volume if the source model is composed of equal-volume elements.

In the case of our model, composed of variable-volume elements, as shown in Fig. 1, the penalizing operator and

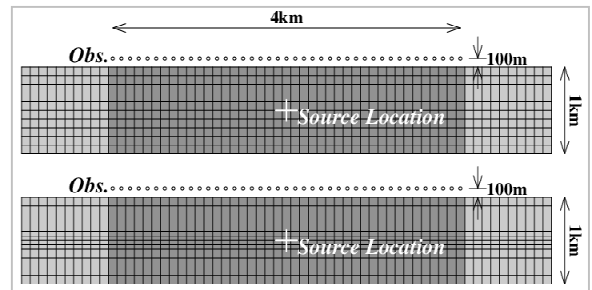


**Fig. 3** Equal-thickness and variable-thickness source layer configurations (section view) for the test analysis against a point source model anomaly. At the centre, a source magnetic moment of  $10^9 \text{ Am}^2$  was assumed in the same direction as the ambient magnetic field,  $45^\circ$  inclination and  $-7^\circ$  declination, which causes a  $-235$  to  $+560 \text{ nT}$  anomaly at the observation points.

the regularizing factor should be

$$\mathbf{B} = \text{diag} \left\{ \sqrt{\frac{v_i}{s_i^2 + \delta^2}} \right\}, \quad (9)$$

$$R = (\mathbf{B}\mathbf{s})^\top (\mathbf{B}\mathbf{s}) = \sum_i \frac{v_i s_i^2}{s_i^2 + \delta^2}, \quad (10)$$

where  $v_i$  is the volume of the  $i$ -th source body.

### Parameter Scaling

As mentioned above, the CG solution of the underdetermined problem falls into a minimum Euclidean norm solution. This implies that different scaling of parameter values results in different results of subsurface imaging, because the scaling factor directly affects the norm of parameter values. Due to the minimum norm condition, there is the tendency that only the parameters ( $s_i$ ) having a larger contribution on the observation ( $f$ ), or shallower source elements unless artificially scaled, are selectively used to account for the observation. To compensate for this situation, Li and Oldenburg (1996) and Pilkington (1997) applied a depth scaling (weighting) as a factor related to the source depth from the surface.

Using the scaling coefficients  $\mathbf{C} = \text{diag}\{c_i\}$ ,  $\mathbf{C}^{-1} = \text{diag}\{1/c_i\}$ , the parameter  $\mathbf{s}$  is scaled into  $\mathbf{s}' = \mathbf{C}^{-1}\mathbf{s}$ . Then Equations (2) and (4) are respectively reduced to

$$\mathbf{f} = \mathbf{A}\mathbf{C}\mathbf{s}', \quad (11)$$

$$\mathbf{C}\mathbf{A}^\top \mathbf{f} = \mathbf{C}\mathbf{A}^\top \mathbf{A}\mathbf{C}\mathbf{s}'. \quad (12)$$

As the source parameters generally should have equal importance in recovering source structure imaging, the optimal scaling factor will not depend on the depth but on the configuration of the source-observation relationship. This relationship is reflected in the normal Equation (12), and we use the scaling so that the diagonal components of the matrix  $\mathbf{C}\mathbf{A}^\top \mathbf{A}\mathbf{C}$  become a common value (such as unity), as adopted by Portniaguine and Zhdanov (2002). Here, we call this 'parameter auto-scaling'.

### PRIMITIVE MODEL PRACTICE

In order to understand the characteristic behaviour of the aforementioned regularization methods and parameter scaling, we performed analyses using point source model data, which is completely equivalent to a spherical body source centred at the point. In this model practice, an

analysis model with a flat top surface was adopted for simplicity. Two types of layer configurations (shown in Fig. 3), equal and variable thickness source layer configurations, both consisting of  $61 \times 61 \times 10$  source blocks including the surrounding zone, were used. Although the second configuration is not realistic for actual data analysis, its purpose is only to confirm the characteristic behaviour.

Figure 4 shows the results for the equal thickness source layer configuration. Panel (a) is the result with no

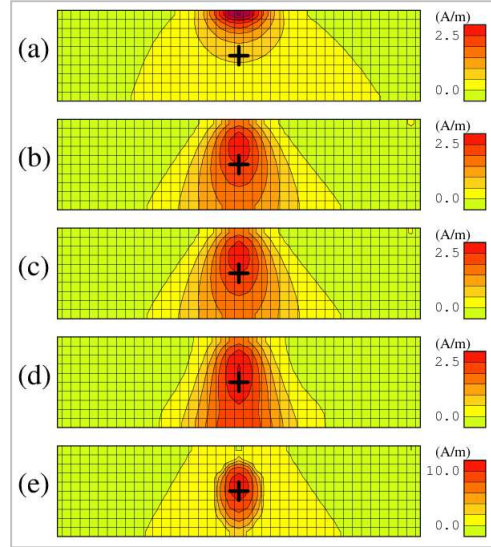


**Fig. 4** Effect of depth scaling and regularization for the equal-thickness source layer configuration. The distribution of magnetization on the central N-S vertical section is shown. (a) result with no parameter scaling and (b)–(e) results of parameter auto-scaling; and (a),(b) without regularization, (c) with minimum norm regularization, (d) with smoothness (minimum roughness) regularization, and (e) with compactness regularization. The black cross indicates the model source location.

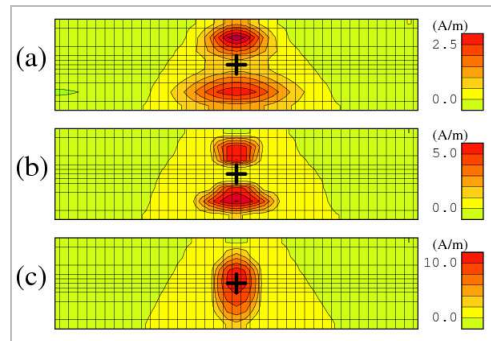


**Fig. 5** Effect of variable volume of source elements. The distribution of magnetization on the central NS vertical section calculated for the three cases of (a) minimum norm regularization with depth scaling but without volume scaling, (b) minimization of the number of effective sources, and (c) minimization of the total volume of the effective sources. The black cross indicates the model source location.

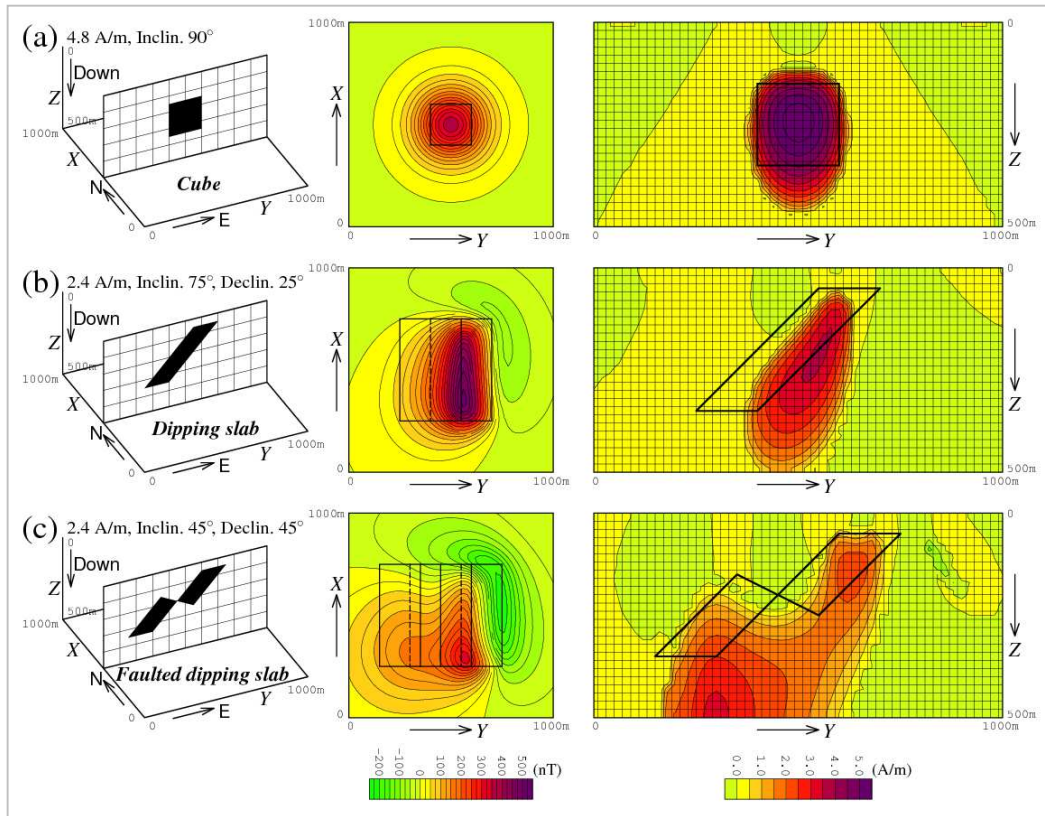
parameter (depth) scaling, and the others are results with parameter auto-scaling; and (a)–(b) are results with no regularization, (c) with minimum norm regularization, (d) with smoothness (minimum roughness) regularization, and (e) with compactness regularization. The cross mark in each panel indicates the actual source location. The necessity of depth scaling is obvious, and the depth of the centre of magnetization (mass) in panels (b)–(e) is near the cross mark. The close similarity of (b) and (c) depicts that no regularization is actually equivalent to the minimum norm regularization. In contrast, the result of compactness regularization (minimizing the number of effective sources) provides a good image for the subsurface structure.

Figure 5 shows the results for the variable thickness source layer configuration. Panel (a) is the result of minimum norm regularization with depth scaling but not volume scaling, whereas (b) and (c) are the results of regularizations minimizing the number and the total

volume of effective sources, respectively. It is obvious that scaling for the variable volume of the source element is essential to getting a reasonable result. Volume scaling for compactness regularization is easily implemented by using Equations (9) and (10) in place of Equations (7) and (8).

## SYNTHETIC MODEL EXAMPLES

Next, the minimum effective volume regularization algorithm was applied to synthetic model examples. Figure 6 shows three models that are nearly the same as those discussed by Portniaguine and Zhdanov (2002);  $71 \times 71 \times 25$  source blocks, including the surrounding zone, were assumed. The result is generally similar to their result. The horizontal locations of the source bodies are recovered well, but the recovery of vertical structure is inaccurate toward the deeper portion. This might indicate a limitation from the inherent non-uniqueness. Nevertheless, the results of compact inversion methods



**Fig. 6** Synthetic example of 3D imaging for the models of (a) cube, (b) dipping slab, and (c) faulted dipping slab, similar to those discussed by Portniaguine and Zhdanov (2002).

Left: sketch of source body at the E-W vertical section; Centre: synthetic magnetic anomaly (calculated for the magnetization and geomagnetic field direction parameters described in the left panel) with horizontal outline of the source body; Right: result of compact inversion (imaging by minimum effective volume regularization) at the E-W vertical section crossing the centre of the source body. For each model, the synthetic magnetic anomaly distribution (centre panel) was regarded as the observation and was put into the process to obtain a 3D image of subsurface magnetization, only one typical section of which is illustrated in the right panel. These analyses are based on a priori knowledge of the magnetization direction but without any source intensity distribution for the initial condition (starting from parameter values of all zero).

can be informative enough to interpret magnetic anomalies in terms of 3D structure. However, it is not so easy to interpret the faulted structure of the third case from the appearance of the anomaly.

In the process of iterative solution of the problem, the trade-off parameter  $e$  plays an important role. To minimize the misfit term,  $e$  is decreased during the process. However, if  $e$  is decreased too fast, the regularization term becomes ineffective and the solution resembles the minimum norm solution. To ensure that the solution becomes compact, a relatively large value of  $e$  should be maintained for as long as possible.

### APPLICATION TO AEROMAGNETIC FIELD DATA OF THE OTOGE CAULDRON

#### Otoge Cauldron

A ring-shaped geological structure occurs in the Shitara area, Central Japan. From geological and petrological studies, Takada (1987) reported the structure of the Middle Miocene Otoge volcanic complex to be a cauldron structure with post-cauldron intrusive dike and sheet swarms, and Geshi (2003, 2005) discussed the evolution of the structure. Figure 7 illustrates the geology of the area. The volcanic activities of the Otoge igneous complex are divided into two stages, i.e., the cauldron-forming stage of eruption of the Otoge pyroclastic rocks with which the Otoge cauldron is filled, and the post-cauldron stage of the intrusive Otoge cone sheets, Otoge stock, and Shitara central dike swarm. The distribution and dip of the Otoge cone sheets suggest the depth to the post-cauldron-activity magma reservoir (Fig. 8).

A helicopter-borne magnetic survey was conducted in this area in 2003 at a flying altitude of 300 m above the ground and a line spacing of 500 m using a stinger-type sensor mount. Although only limited data were acquired for the purpose of mapping a rather small area (because this survey was aimed only at the verification of newly developed equipment), a typical magnetic anomaly pattern for the ring structure was revealed.

#### 3D imaging

These magnetic anomaly data were used in 3D imaging analysis with compact regularization after removing a linear regional trend. A 10-layer source model of constant burial depth slicing was used, and a total of about 13 thousand data (100-m mesh) as the observation was used to estimate 16 times as many unknown

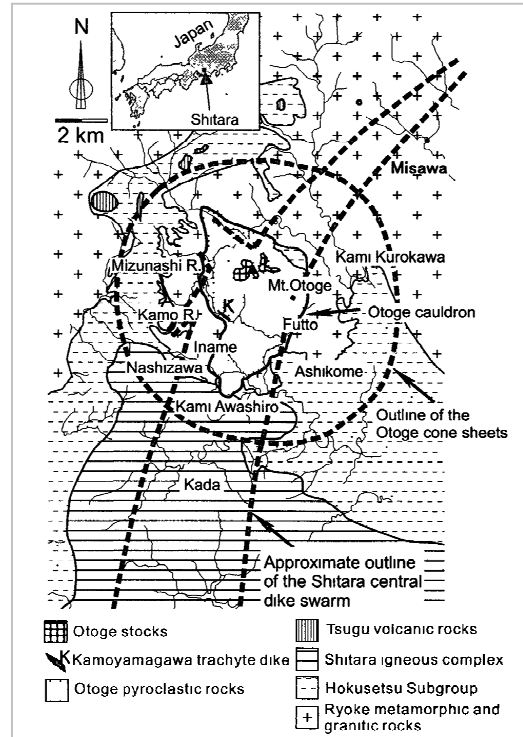


Fig. 7 Geologic outline of the Otoge volcanic complex (after Takada, 1987 and Geshi, 2003, ©Geol. Soc. Japan).

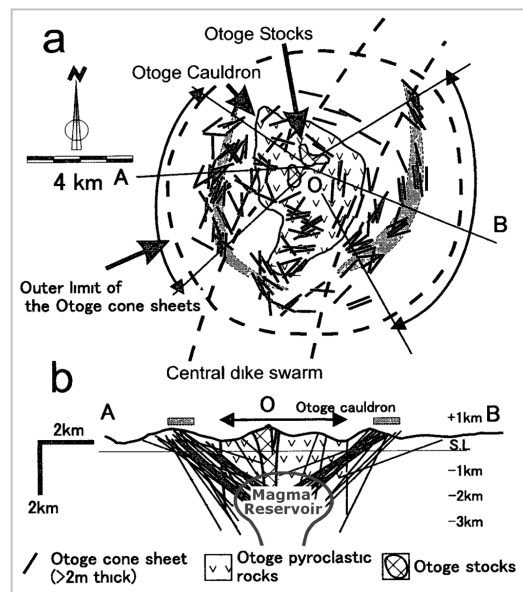


Fig. 8 Distribution (a) and cross section (b) of the Otoge cone sheets (after Geshi, 2003, ©Geol. Soc. Japan). The presumed location of magma reservoir is added.

parameters (including the surrounding zone). Here, a magnetization direction that is the same as the present geomagnetic field was assumed from the appearance of the magnetic anomaly pattern. The starting model (initial guess) of the analysis is the null source (all zero magnetization parameter values).

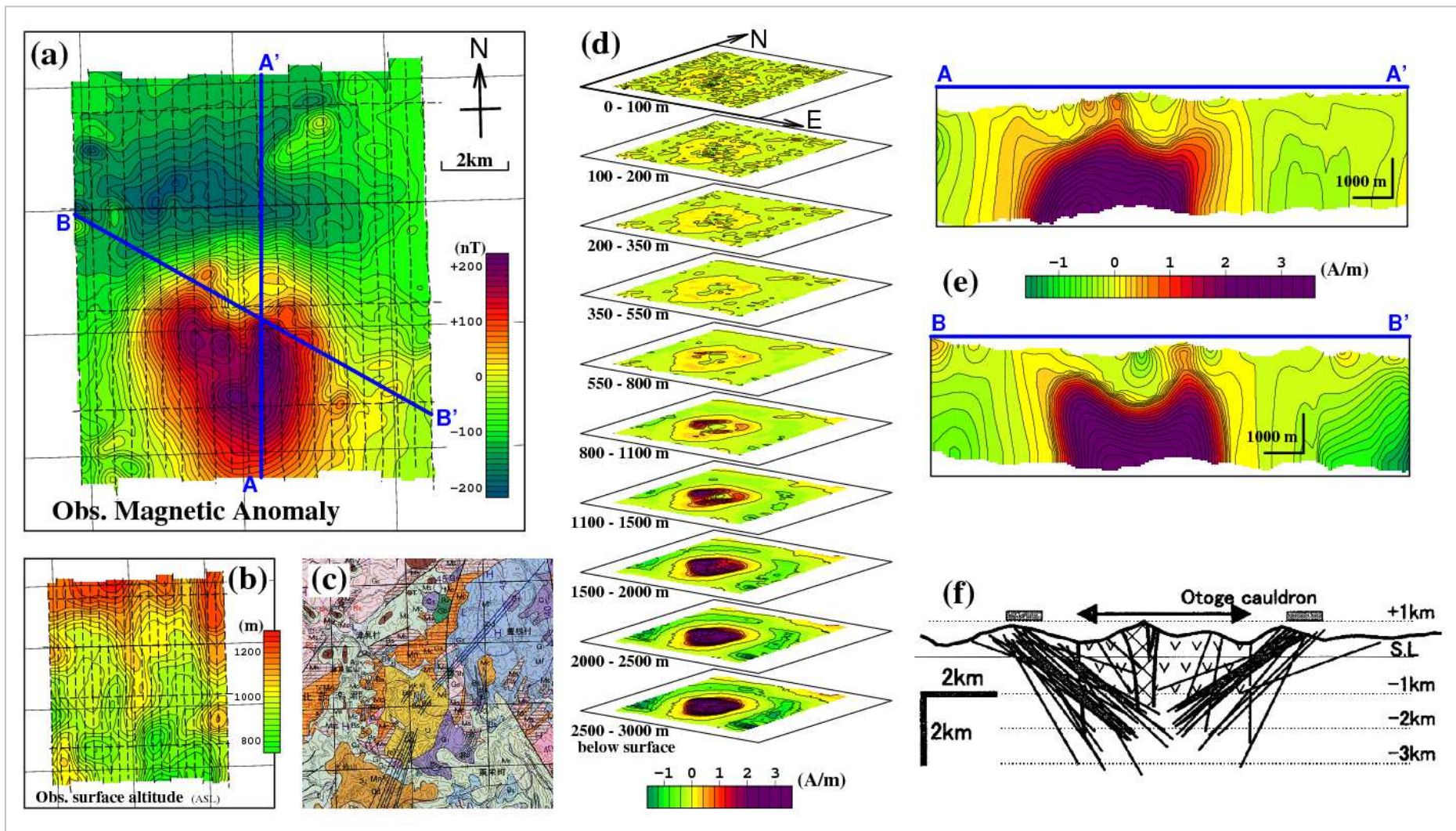


Fig. 9 3D imaging analysis of aeromagnetic anomalies in the Otoge cauldron, Shitara area.

The aeromagnetic anomaly (a) reduced to a smooth reduction surface (b) was put into the 3D imaging process with the minimum effective source volume regularization. The result is shown as a magnetization distribution on each depth-range layer (d) and in two vertical sections (e) along the blue lines A–A' and B–B' shown in (a).

A geologic map of the area (c) (Makimoto *et al.*, 2004) and a cross section view of the Otoge cone sheets (f) (same as in Fig. 8b) are shown for reference.

The observed magnetic anomalies, altitudes, surface geology of the area, and the result of analysis are summarized in Fig. 9. Panel (b) shows the smoothed version of the actual observation altitudes, ranging from 660–1330 m above sea level, to which the observed magnetic anomalies were reduced with the equivalent source method (Nakatsuka and Okuma, 2006a), and the result (a) (regular mesh in horizontal) of the reduction was put into the 3D imaging analysis. This process might be useful for removing the non-harmonic noise component and making the data distribution uniform. The iterative process of the CG method was continued until the 75th loop, when the RMS misfit decreased to 0.18 nT. The results of the analysis are shown as the estimated magnetization distribution on each layer (d) and on two vertical sections (e) marked by the blue lines in panel (a). The range of the drawings of panels (a), (b), and (c) and each parallelogram in (d) are the same, although the scale is different.

## Results

Panel (d) of Fig. 9 clearly manifests the existence of a high magnetization body at the depth of 2000 m and below, and it is easily correlated with the magma reservoir predicted from the geology (Fig. 8). Its shape is almost a vertical cylinder with a diameter of about 5 km. The shallower extension of the magma reservoir branches into two parts (WNW and ESE), and the massive body rises to a depth of 800 m at the western branch. The existence of these two branches seems to be related to the cone sheet activity with a non-axisymmetric distribution (Fig. 8a).

The vertical sections in panel (e) pass through the location of the Otoge stocks, which correspond to the higher magnetization (orange color) parts ascending from the magma reservoir.

Although other features of the result are not remarkable in the illustration, there is a ring-shaped higher magnetization part at shallower depths (yellow color, < 800 m) in panel (d), and the extensions of higher magnetization at the shoulders of the magma reservoir are noticed in panel (e). These patterns are generally consistent with the distribution of the Otoge cone sheets. As the thicknesses of the cone sheets are mostly less than 3 m (Takada, 1987), the bulk magnetization averaged within the analysis element might have been decreased.

As the analysis was performed with a model of depth range of 0–3000 m, there is a possibility that the effect of an actual magnetic structure deeper than 3000 m may distort the analysis result, especially in the deeper portion. Also, we assumed the source magnetization direction to be the same as the present magnetic field direction because of a lack of rock-magnetic studies of the field. Recently, Lelièvre *et al.* (2009) and Li *et al.* (2010) developed a solution for the problem including significant remanence magnetization. We would like to consider such a situation as the subject of a future study.

## CONCLUSIONS

3D inversion analysis of potential field data has the inherent weakness of non-uniqueness, and it is most important to introduce a valid and reasonable constraint in the analysis model. However, it is often difficult in the practical data handling to select an appropriate constraint because only limited information is available. Hence, it is beneficial to apply the 3D imaging method described above to show one possible result of a rather loose constraint.

We studied regularization methods and parameter scaling in the use of a primitive model. The parameter scaling dependent on the depth is an indispensable factor to recovery of a valid subsurface structure, and the scaling for the volume of the source element is also important if the source model consists of variable-volume elements. For a helicopter-borne survey in a mountainous region, it is appropriate to select automatic scaling of parameters utilizing the property of the matrix itself of the problem.

We developed 3D imaging software applicable to helicopter-borne magnetic surveys in rugged terrain, making use of the regularization of the minimum effective source volume. The software was tested on geologic models to verify its efficiency and applied to aeromagnetic data from the Shitara area.

The results of the aeromagnetic 3D imaging analysis in the Shitara area revealed a quite reasonable subsurface image of the magma reservoir and the Otoge cone sheets and Otoge stocks of the post-cauldron activity, as inferred from geological studies.

## ACKNOWLEDGEMENTS

Parts of this paper were presented at the 9th (2009) and 10th (2011) SEGJ International Symposium. We are

grateful to all who attended the Symposia for their constructive discussion.

## REFERENCES

- Bhattacharyya, B. K., 1964, Magnetic anomalies due to prism-shaped bodies with arbitrary polarization: *Geophysics*, **29**, 517-531. [doi: 10.1190/1.1439386](https://doi.org/10.1190/1.1439386)
- Clark, D. A., 2013, New methods for interpretation of magnetic vector and gradient tensor data II: application to the Mount Leyshon anomaly, Queensland, Australia: *Exploration Geophysics*, **44**, 114-127. [doi: 10.1071/EG12066](https://doi.org/10.1071/EG12066)
- Geshi, N., 2003, Development of the Middle Miocene Otoge volcanic complex, Shitara district, central Japan: *J. Geol. Soc. Japan*, **109**, 580-594. [doi:10.5575/geosoc.109.580](https://doi.org/10.5575/geosoc.109.580)
- Geshi, N., 2005, Structural development of dike swarms controlled by the change of magma supply rate: the cone sheets and parallel dike swarms of Miocene Otoge igneous complex, Central Japan: *J. Volcanol. Geotherm. Res.*, **141**, 267-281. [doi: 10.1016/j.jvolgeores.2004.11.002](https://doi.org/10.1016/j.jvolgeores.2004.11.002)
- Last, B. J., and Kubik, K., 1983, Compact gravity inversion: *Geophysics*, **48**, 713-721. [doi: 10.1190/1.1441501](https://doi.org/10.1190/1.1441501)
- Lelièvre, P. G., and Oldenburg, D. W., 2009, A 3D total magnetization inversion applicable when significant, complicated remanence is present: *Geophysics*, **74**, L21-L30. [doi: 10.1190/1.3103249](https://doi.org/10.1190/1.3103249)
- Li, Y., and Oldenburg, D. W., 1996, 3-D inversion of magnetic data: *Geophysics*, **61**, 394-408. [doi: 10.1190/1.1443968](https://doi.org/10.1190/1.1443968)
- Li, Y., Shearer, S. E., Haney, M. M., and Dannemiller, N., 2010, Comprehensive approaches to 3D inversion of magnetic data affected by remanent magnetization: *Geophysics*, **75**, L1-L11. [doi: 10.1190/1.3294766](https://doi.org/10.1190/1.3294766)
- Makimoto, H., Yamada, N., Mizuno, K., Takada, A., Komazawa, M., and Sudo, S., 2004, *Geological Map of Japan 1:200,000, Toyohashi and Irago Misaki*: Geol. Surv. Japan, AIST. ([https://www.gsj.jp/Map/JP/docs/200k\\_doc/ni53\\_02-03.htm](https://www.gsj.jp/Map/JP/docs/200k_doc/ni53_02-03.htm))
- Nakatsuka, T., 1995, Minimum norm inversion of magnetic anomalies with application to aeromagnetic data in the Tanna area, Central Japan: *J. Geomag. Geoelectr.*, **47**, 295-311. [doi: 10.5636/jgg.47.295](https://doi.org/10.5636/jgg.47.295)
- Nakatsuka, T., and Okuma, S., 2006a, Reduction of geomagnetic anomaly observations from helicopter surveys at varying elevations: *Exploration Geophysics*, **37**, 121-128; *Butsuri-Tansa*, **59**, 121-128; *Mulli-Tansa*, **9**, 121-128. [doi: 10.1071/EG06121](https://doi.org/10.1071/EG06121)
- Nakatsuka, T., and Okuma, S., 2006b, Crossover analysis for the aeromagnetic survey at varying elevations, and its application to extracting temporal magnetic anomaly change: *Butsuri-Tansa (Geophys. Explor.)*, **59**, 449-458. [doi: 10.3124/segj.59.449](https://doi.org/10.3124/segj.59.449)
- Nakatsuka, T., Utsugi, M., Okuma, S., Tanaka, Y., and Hashimoto, T., 2009, Detection of aeromagnetic anomaly change associated with volcanic activity: an application of the generalized mis-tie control method: *Tectonophysics*, **478**, 3-18. [doi: 10.1016/j.tecto.2009.02.018](https://doi.org/10.1016/j.tecto.2009.02.018)
- Okubo, A., Nakatsuka, T., Tanaka, Y., Kagiya, T., and Utsugi, M., 2006, Aeromagnetic constraints on the subsurface structure of the Unzen Graben, Kyushu, Japan: *Earth Planets Space*, **58**, 23-31. (<http://www.terrapub.co.jp/journals/EPS/pdf/2006/5801/58010023.pdf>)
- Okuma, S., Makino, M., and Nakatsuka, T., 1994, Magnetization intensity mapping in and around Izu-Oshima Volcano, Japan: *J. Geomag. Geoelectr.*, **46**, 541-556. [doi: 10.5636/jgg.46.541](https://doi.org/10.5636/jgg.46.541)
- Okuma, S., Stotter, C., Supper, R., Nakatsuka, T., and Furukawa, R., 2009, Aeromagnetic constraints on the subsurface structure of Stromboli Volcano, Aeolian Islands, Italy: *Tectonophysics*, **478**, 19-33. [doi: 10.1016/j.tecto.2009.02.035](https://doi.org/10.1016/j.tecto.2009.02.035)
- Pilkington, M., 1997, 3-D magnetic imaging using conjugate gradients: *Geophysics*, **62**, 1132-1142. [doi: 10.1190/1.1444214](https://doi.org/10.1190/1.1444214)
- Pilkington, M., 2009, 3-D magnetic data-space inversion with sparseness constraints: *Geophysics*, **74**, L7-L15. [doi: 10.1190/1.3026538](https://doi.org/10.1190/1.3026538)
- Portniaguine, O., and Zhdanov, M. S., 1999, Focusing geophysical inversion images: *Geophysics*, **64**, 874-887. [doi: 10.1190/1.1444596](https://doi.org/10.1190/1.1444596)
- Portniaguine, O., and Zhdanov, M. S., 2002, 3-D magnetic inversion with data compression and image focusing: *Geophysics*, **67**, 1532-1541. [doi: 10.1190/1.1512749](https://doi.org/10.1190/1.1512749)
- Silva, J. B. C., Oliveira, F. S., Barbosa, V. C. F., and Campos Velho, H. F., 2007, Apparent-density mapping using entropic regularization: *Geophysics*, **72**, I51-I60. [doi: 10.1190/1.2732557](https://doi.org/10.1190/1.2732557)
- Takada, A., 1987, Structure of a cauldron in the Otoge Ring Complex, Shitara district, Aichi Prefecture, central Japan: *J. Geol. Soc. Japan*, **93**, 107-120. [doi:10.5575/geosoc.93.107](https://doi.org/10.5575/geosoc.93.107)
- Uchida, T., 1993, Smooth 2-D inversion for magnetotelluric data based on statistical criterion ABIC: *J. Geomag. Geoelectr.*, **45**, 841-858. [doi: 10.5636/jgg.45.841](https://doi.org/10.5636/jgg.45.841)